

## Dielectrophoretic manipulation of macromolecules: The electric field

D. S. Clague\* and E. K. Wheeler†

Center for Microtechnology/EETD, L-223, Lawrence Livermore National Laboratory, Livermore, California 94550

(Received 14 March 2001; published 18 July 2001)

The use of dielectrophoresis is fast becoming a proven technique for manipulating particles and macromolecules in microfluidic systems. Here an analytic solution for the gradient in the electric field strength,  $\nabla \cdot (\mathbf{E} \cdot \mathbf{E})$ , produced by a two-dimensional array of parallel electrodes is derived using the method of Green's functions. The boundary condition for the potential between electrodes is estimated by using a linear approximation. While the Green's function used here is somewhat different from Wang *et al.*, J. Phys. D **29**, 1649 (1996), the resulting analytic expression for the potential field is in exact agreement with their result. Selected results for equispaced electrodes with equal widths are compared with Wang *et al.*, J. Phys. D **29**, 1649 (1996). The analytic solution is employed to study the effects of electrode spacing and electrode width on the gradient in electric field intensity. Results show that the magnitude in the gradient in the electric field intensity exhibited the expected dependence on the applied voltage; however, the dependence on electrode width was found to be on the order of the electrode width squared. Results to explore the effects of electrode spacing show that as the spacing is reduced below two electrode widths the magnitude of the gradient increases exponentially.

DOI: 10.1103/PhysRevE.64.026605

PACS number(s): 41.20.-q, 46.25.Cc, 89.75.Da

### I. INTRODUCTION

Dielectrophoresis (DEP) is a phenomenon by which a non-uniform electric field induces a net force on a polarizable particle (or macromolecule). As described by Pohl [1], the field can be produced by either a direct current (dc) or alternating current (ac). The only requirement is that the field be nonuniform. This field nonuniformity causes an imbalance in the Lorenz forces produced at the (natural or induced) particle poles so that the resultant net forces,  $\mathbf{F} = \mathbf{E} q$ , is nonzero and causes particle motion. Depending on the relative difference between the complex dielectric properties of the suspended particle and the suspending medium [2], this net force causes particles to be either attracted or repulsed from regions of high field intensity. The first order or dipole contribution to the dielectrophoretic force [1–5] is given by

$$F_{DEP} = 2 \pi a^3 \epsilon_m^* K(\epsilon_p^*, \epsilon_m^*) \nabla(\mathbf{E} \cdot \mathbf{E}). \quad (1)$$

Here  $\mathbf{E}$  is the electric field,  $a$  is the particle radius,  $K(\epsilon_p^*, \epsilon_m^*)$  is the Clausius-Mossotti factor, and  $\epsilon_p^*$  and  $\epsilon_m^*$  are the complex permittivities of the particle and the suspending medium, respectively. It should be noted here that Eq. (1) is the time-averaged force [3], and for the work presented in this communication, we focus on standing wave dielectrophoresis [5].

The permittivity and conductivity of the target species and suspending medium must be determined through experimental means, and in some cases, these data are available in the open literature [6,7]. Aside from experimental determination of the complex permittivities, an analytic solution for the electric field and the gradient in the electric field intensity have been the most difficult unknown to obtain. Therefore,

we are interested in developing an analytic solution for the electric field and the gradient in the electric field intensity produced by a parallel array of electrodes. Past efforts to solve this problem include: the use of commercial finite element methods (Maxwell<sup>TM</sup>), the charge density method [4], Green's theorem [5], and the Green's function for a line source with conformal mapping [8]. Each of these approaches are briefly discussed below.

In the charge density method, each electrode is subdivided into sufficiently small domains so that the surface charge density in each subdomain can be considered constant [4]. By using the fundamental relationship between the surface charge density to the potential [4], one can determine the field potential above the electrode array. From the resulting potential, one can obtain all of the desired field quantities, that is,  $\mathbf{E}$  and  $\nabla(\mathbf{E} \cdot \mathbf{E})$ , see Wang *et al.* [4] for details. The only disadvantage to this approach is the necessity of solving many simultaneous equations, that is, each subdomain problem, to construct the complete solution. This process can be computationally expensive.

In the Green's theorem approach of Wang *et al.* [5], the problem of interest is reciprocally related to a known, tractable problem using Green's theorem. By doing this they construct a three-dimensional Green's function (or propagator) that enables the prediction of the potential above the electrode plane as a function of the surface potential [5]. The only limitation of this approach is that the functionality of the surface potential in the gaps between electrodes must be assumed. Wang *et al.* demonstrate their approach using a two-dimensional array of parallel electrodes with a linear approximation for the surface potential in the gaps between electrodes. While this is clearly an approximation, they show that at a height of  $10 \mu\text{m}$  above the electrode array for an applied voltage of  $1 V_{rms}$  that their result only over-predicts the potential predicted by the charge density method by approximately 5%. As stated by Wang *et al.* [5], the primary advantages of the Green's theorem approach over other ap-

\*Author to whom correspondence should be directed. Email address: clague1@llnl.gov

†Email address: wheeler16@llnl.gov

proaches is that it is accurate and the analytic form yields rapid results [5]. In later parts of their work, they introduce and use higher order, nonlinear approximations for the surface, gap potential.

The Green's function approach of Garcia and Clague [8] uses the Green's function for a line source [9] to represent each electrode. The Green's function goes as  $-2 \ln(r)$ , where  $r$  is the radial position relative the source. In their analysis, the electrodes are defined as an array of strip electrodes. The strip array is then mapped onto an array of cylinders where the potential and field are produced by summing the contribution from each line source representing the individual cylinders. From this they construct a solution for the potential and the resulting  $\mathbf{E}$  field, which they then map back to cartesian coordinates to obtain a solution for a parallel array of strip electrodes. Like the charge density method, this approach requires no knowledge of the surface boundary condition in the gap between electrodes; however, because  $\ln(r)$  dependence does change sign when  $r$  transitions from less than 1 to greater than 1,  $r$  must be normalized by a characteristic length scale or combination of length scales descriptive of the system, e.g., the location of the ground plane. The magnitude of the resulting solution to  $\nabla(\mathbf{E} \cdot \mathbf{E})$  is influenced by the choice of this length scale. Nonetheless, their approach is instructive and useful for further analysis of additional electrode configurations.

In this study, we use the half-plane Green's function [9], and a linear approximation for the surface potential in the gaps between electrodes [5], to construct our solution. The half plane Green's function is two-dimensional and functionally different from the Green's function derived by Wang *et al.* [5]; however, in principle, for an identical configuration of electrodes under the same conditions, our solution should be in exact agreement with Wang *et al.* [5]. In addition, we do not take into account the variation in field properties due the presence of multiple particles.

In Sec. II, we present the approach used to derive the potential field, and the resulting analytic solutions for the potential field, electric field and the gradient in the electric field intensity. The components of the gradient of the electric field intensity are presented as a function of the height above an electrode array in Sec. III. In addition, results for variations in electrode width, spacing and the applied voltage are also presented in Sec. III. Finally, in Sec. IV, the important conclusions are discussed.

## II. THEORETICAL BACKGROUND

The analysis here is for parallel electrode arrays where the in-plane direction can be considered of infinite length relative to the other two dimensions. As a consequence, the electrode array can be considered a two-dimensional system. The resulting configuration is described in Fig. 1.

As shown above, the location of the  $k$ th midpoint between electrode pairs is denoted as  $\lambda_k$ ; the center-to-center to center spacing between the electrodes is  $2d$ ; the electrode width is  $w$ ; and, the leading and trailing edges of the  $j$ th electrode are given by  $a_j$  and  $b_j$ , respectively.

To solve for the potential field produced by the electrode

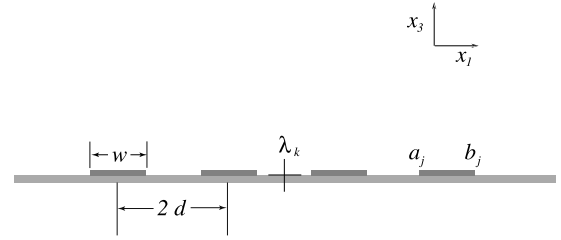


FIG. 1. Planar electrode array: A two-dimensional array of equi-width and equispaced electrodes. The electrode width is  $w$  and the leading and trailing edges of the  $j$ th electrode are  $a_j$  and  $b_j$ , respectively.  $\lambda_k$  denotes the location of the  $k$ th midpoint between two adjacent electrodes.

array, we make use of the upper half-plane Green's function for the potential above a plane (cf. Eq. 6.3.3 in Ref. [9]):

$$G(x_1, x_3 | \xi) = \frac{x_3 / \pi}{(x_1 - \xi)^2 + x_3^2}. \quad (2)$$

Here  $x_3$  is the vertical position above the plane;  $x_1$  is horizontal position along the electrode plane; and  $\xi$  is the position of the surface potential in the  $x_1$  direction on the electrode plane. To obtain an expression for the potential above the electrode plane, we perform a piecewise integration of the product of Eq. (2) and the appropriate surface potential boundary condition along the entire surface of electrode plane,

$$\psi(x_1, x_3) = \int_{-\infty}^{\infty} G(x_1, x_3 | \xi) \psi_s(\xi) d\xi. \quad (3)$$

The surface potential  $\psi_s(\xi)$  is a function of the surface coordinate  $\xi$ . On the electrodes, we apply an ac voltage, where the phase is changed by increments of  $\pi/2$  consecutively for each electrode in the array. The applied potential to the  $j$ th electrode is given as

$$\psi_e(\xi) = V_0 \cos\left(\omega t + \frac{2\pi j}{n}\right). \quad (4)$$

$V_0$  is the magnitude of the applied rms voltage,  $\omega$  is the frequency of the applied signal,  $j$  is the electrode identification, and  $n$  is the mode.

For the analysis to follow, we are primarily interested in stationary phase DEP; therefore,  $n$  will be set to 2. It should be pointed out, however, that the solution derived below is general and could be used useful to study traveling wave DEP,  $n=4$ , as well.

To describe the surface potential in the gaps between electrodes we use a linear approximation as described in Ref. [5], or

$$\psi_g(\xi) = V_0 \left( \left[ \frac{\cos_{j+1} - \cos_j}{2d - w} \right] [\xi - \{\lambda_k - d + w/2\}] + \cos_j \right), \quad (5)$$

where  $\phi_g$  is the surface potential in the gap, and  $\lambda_k$  still denotes the midpoint between the  $k$ th pair of electrodes. All

other terms are as described above.  $\cos_j$  is simply  $\cos(\omega t + 2\pi j/n)$ , and  $\cos_{j+1}$  is  $\cos_j$  evaluated at  $j+1$ . While this is clearly an approximation of reality, Wang *et al.* [5] have shown that use of this boundary condition, Eq. (5), yields results that are in excellent agreement with results produced by rigorous application of the charge density method.

### The potential field

Substituting the surface potentials given in Eqs. (4) and (5) into Eq. (3) and integrating yields the following solution for the electric potential above the electrode array shown in Fig. 1:

$$\begin{aligned} \psi(x_1, x_3) = & -\frac{1}{\pi} \sum_{j=1}^N \psi_e \left( \arctan \left[ \frac{x_1 - b_j}{x_3 - x_{3_0}} \right] \right. \\ & \left. - \arctan \left[ \frac{x_1 - a_j}{x_3 - x_{3_0}} \right] \right) + \frac{1}{\pi} \sum_{j=1}^{N-1} \left\{ -\psi_g(x_1) \right. \\ & \times \left( \arctan \left[ \frac{x_1 - a_{j+1}}{x_3 - x_{3_0}} \right] - \arctan \left[ \frac{x_1 - b_j}{x_3 - x_{3_0}} \right] \right) \\ & + \frac{C_2(x_3 - x_{3_0})}{2} \ln \left( 1 + \left[ \frac{x_1 - a_{j+1}}{x_3 - x_{3_0}} \right]^2 \right) \\ & \left. - \ln \left( 1 + \left[ \frac{x_1 - b_j}{x_3 - x_{3_0}} \right]^2 \right) \right\}. \end{aligned} \quad (6)$$

Here  $x_{3_0}$  locates the height of the electrode plane. The constants  $C_1$ ,  $C_2$ , and  $C_3$  form the gap surface potential given in Eq. (5), i.e.,  $\psi_g(x_1) = C_1 + C_2 x_1 + C_3$ . Specifically,  $C_1 = V_0 \cos_j$ ,  $C_2 = V_0(\cos_{j+1} - \cos_j)/2d - w$ , and  $C_3 = -(\lambda_k - d + w/2)C_2$ . While the potential given above in Eq. (6) results from the use of the Green's function given in Eq. (2), the solution given above is identical to Wang *et al.* [5].

As shown in Eq. (1), the DEP force is proportional to the gradient in the electric field intensity,  $\nabla(\mathbf{E} \cdot \mathbf{E})$ ; therefore, we need to develop analytic expressions for the partial derivatives of the appropriate terms. Before doing this, however, it is instructive to look at this gradient,  $\nabla(\mathbf{E} \cdot \mathbf{E})$ , in index notation, or,

$$\frac{\partial}{\partial x_m} E_r E_r = 2E_r \frac{\partial E_r}{\partial x_m}, \quad (7)$$

where  $r$  and  $m$  are the directional indices. It is clear that to derive expressions for the gradient we need only obtain the appropriate partial derivatives of  $E_1$  and  $E_3$ . All of the terms necessary to construct  $\nabla(\mathbf{E} \cdot \mathbf{E})$  are given in the Appendix. While our starting point, Eq. (2), differs from Wang *et al.* [5], it can be shown mathematically that we arrive at identical results for the electric potential and the resulting terms that form the gradient in the electric field intensity. The two independent results serve to confirm each effort.

In the section to follow, we show results for  $\nabla(\mathbf{E} \cdot \mathbf{E})$  for various electrode widths, spacings, and applied voltages.

## III. RESULTS

The electric field intensity generated by a parallel array of interdigitated electrodes produces sufficient dielectrophoretic forces to manipulate colloidal particles and macromolecules in microflows. Because the DEP force is proportional to the gradient in the electric field intensity, it is instructive to look at the components of the gradient in the electric field intensity to gain a better intuition into the forces acting on target species. In this section, we present surface plots of the electric field intensity and the components of the gradient in the intensity. In the sections below, we present results from studies that explore variations in electrode width, spacing, and applied voltage. These studies were chosen to assist device designers who employ parallel arrays of electrodes to produce dielectrophoretic forces to manipulate particulate species in microfluidic devices.

### A. The electric field intensity and its gradients

The DEP force is a function of the frequency dependent, complex permittivities of the target species and the suspending fluid, the particle radius and the time-averaged gradient in the electric field intensity [2,5], see Eq. (1). This force can be used to either levitate (negative DEP) or facilitate capture (positive DEP) of target species [2]. When using negative DEP, one can use an imposed flow field and separate species based on differences in dielectric properties and effective radii [6]. Specifically, particles of differing properties are levitated to different positions in the flow field and separations occur due to variations in particle velocity. When using positive DEP, the goal is to draw target species to the electrode array surface. Positive DEP can also be used to accomplish desired separations by directing target species into a particular branch at a microchannel junction or by actually capturing the target species on the surface of the electrode array. In the latter example, the vertical component of the DEP force must be sufficient to draw the desired species to the array surface, and the component parallel to the flow must be sufficient to balance the hydrodynamic forces acting on the target species. Like negative DEP, positive DEP separations are effected based on differences in complex permittivities and species radii. To provide greater intuition into the nature of electric field intensity and the gradients in the electric field intensity, we present surface plots of the electric field intensity and the resulting components of the gradient in the electric field intensity.

Shown in Fig. 2 is a surface plot of the electric field intensity produced by the two central electrodes in an array of 20 parallel, equispaced electrodes. In Fig. 2, the electrode width,  $w$ , and edge-to-edge gap between electrodes,  $s = 2d - w$ , are both  $20 \mu\text{m}$ . The applied voltage is  $5 V_{rms}$ , and the sign of the applied voltage on each adjacent electrode is out of phase by  $90^\circ$ . The electric field intensity is sampled at vertical positions that range from 1 to  $30 \mu\text{m}$  above the electrode array. The electrode edges (electrodes not shown) are located at  $-30 \mu\text{m}$ ,  $-10 \mu\text{m}$ ,  $10 \mu\text{m}$  and  $30 \mu\text{m}$  for the two electrodes chosen. Also, it should be noted that we use the time-averaged electric field [2,5]. As a result, the frequency of the applied field is accounted for only through

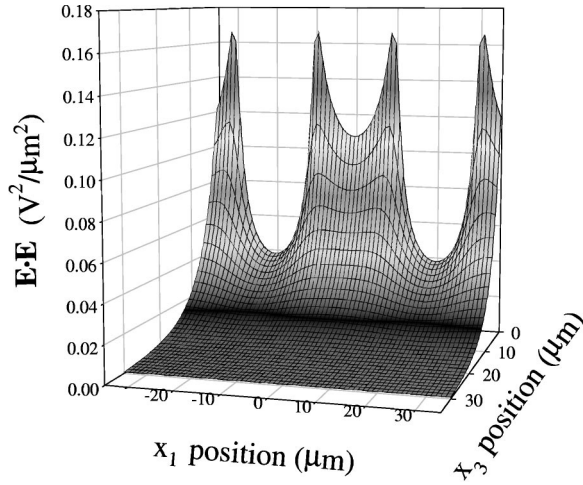


FIG. 2. Electric field intensity  $\mathbf{E} \cdot \mathbf{E}$  above an electrode array. The applied electric field is  $5 V_{rms}$  with an excitation frequency of 2000 Hz. The electrode array is made up of 20 parallel electrodes of infinitesimal thickness with an equal width and gap of  $20 \mu\text{m}$ .

the complex permittivities of the target species and the suspending medium, see Eq. (1).

The electric field intensity maxima, or the sharp peaks, occur near the electrode edges. The slope of these peaks show that when a target species is near the surface of the electrode array the  $x_1$  component of the gradient in the electric field intensity will either resist or augment particle convective transport depending on the particle position relative to the electrode edge. Furthermore, as the test position is moved away from the surface of the electrode array, the electric field intensity drops-off rapidly in an exponential-like fashion; hence, one could also expect a sharp gradient in the  $x_3$  direction near electrode edges. This component of the gradient provides the driving force to effect the desired vertical positioning of target species.

In the context of dielectrophoresis, we are interested in the components of the gradient in the electric field intensity. Shown in Figs. 3 and 4 are surface plots of the  $x_1$  and  $x_3$  components of the gradient in the electric field intensity, respectively. Shown in Fig. 3 is the  $x_1$  component of the gradient in the electric field intensity. The applied voltage is  $5 V_{rms}$ . The sample heights above the electrode array range from 1 to  $30 \mu\text{m}$ . The sharpest fluctuations of this component of the gradient occur near the edges of each electrode, and the sign changes as the test position moves from the leading to the trailing edge of the electrode, see Fig. 2. Specifically, the  $x_1$  component of the DEP force always points toward the electrode edges. In general, this is consistent with experimental observation [10]. For the electrode configuration under investigation in this work, it is this component that must be large enough to overcome the  $x_1$  component of the hydrodynamic force to achieve particle capture.

In Fig. 4, we present the vertical or  $x_3$  component of the gradient in the electric field intensity. The electrode configuration, the applied voltage and the test heights are identical to the conditions used in Fig. 3. As with the  $x_1$  component of the gradient in the electric field intensity, the most dramatic changes in the  $x_3$  component of the gradient occur near the

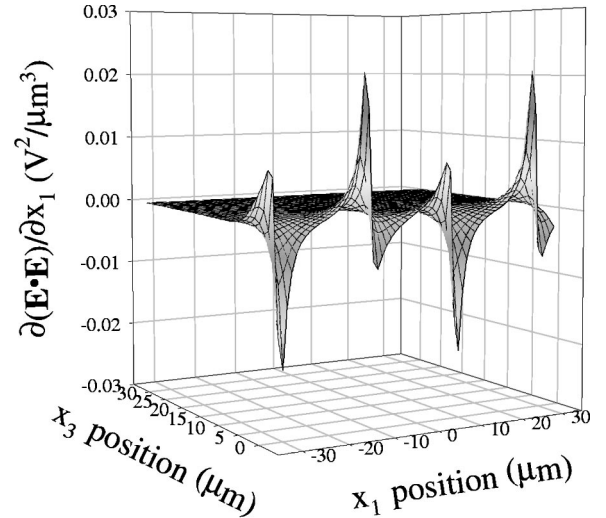


FIG. 3. The  $x_1$  component of the gradient in electric field intensity. The applied voltage is  $5 V_{rms}$ . The electrode array is made up of 20 parallel electrodes of infinitesimal thickness. The width and edge-to-edge spacing between electrodes are both fixed at  $20 \mu\text{m}$ .

edges of each electrode; however, the sign of the  $x_3$  component is always negative and points toward the electrode edges. Depending on the sign of the Clausius-Mossotti factor in Eq. (1), the  $x_3$  component of the gradient in the electric field intensity will either cause levitation or capture. In the case of particle capture, it is this component of the DEP force that must overcome hydrodynamic lift effects [11] to hold the target species at the surface of the electrode array.

## B. Dependence on applied voltage and electrode width

In this section, we explore the dependence of the gradient in the electric field intensity on changes in electrode width, where the spacing  $s$  is equal to the width, and changes in the amplitude of the applied voltage. To guide our intuition, it is instructive to make an order of magnitude estimate of Eq. (1)

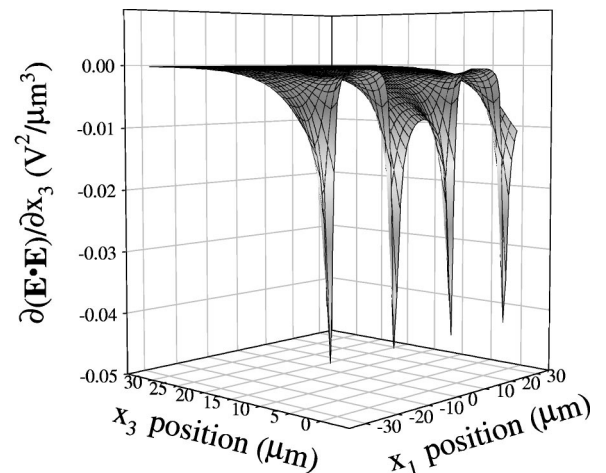


FIG. 4. The  $x_3$  component gradient in electric field intensity. The applied voltage is  $5 V_{rms}$ . The electrode array is made up of 20 parallel electrodes of infinitesimal thickness with a width and edge-to-edge spacing between electrodes of  $20 \mu\text{m}$ .

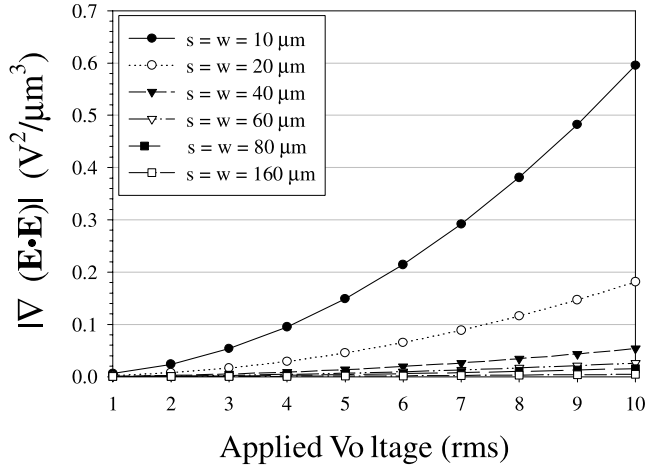


FIG. 5. Gradient in electric field intensity as a function of applied voltage. The electrode widths  $w$  with equal spacing  $s$  are  $20 \mu\text{m}$ ,  $40 \mu\text{m}$ ,  $60 \mu\text{m}$ , and  $80 \mu\text{m}$  for each data set. The applied voltages range from 1 to  $10 V_{rms}$ .

to predict the expected dependencies. By making all length scales in Eq. (1) dimensionless with the particle radius  $a$ , the magnitude in the DEP force scales [12] as

$$|F_{DEP}| \propto \frac{V^2}{L_e^3}. \quad (8)$$

$V$  is the amplitude of the applied voltage, and  $L_e$  is a length scale for a given electrode in the array. For the electrode configuration shown in Fig. 1, the characteristic length scales are assumed to be the width  $w$  of an individual electrode, and the height  $h$  above the array. In figures, we explore the dependence of the gradient in the electric field intensity, and the DEP force, on these parameters.

In Fig. 5, the gradient in the electric field intensity, which is proportional to the DEP force, is plotted as a function of the applied voltages for different electrode widths.

Over the range of voltages sampled, the data were curve fit to a power law. For all voltages and electrode widths tested, the exponent found from fitting the data revealed a squared dependence of the DEP force on the applied voltage with a correlation coefficient of 1,

$$|\nabla(\mathbf{E} \cdot \mathbf{E})| \sim V^2. \quad (9)$$

This result is consistent with the scaling estimate in Eq. (8) and the analytic expressions for the components of the gradient in the electric field intensity given in the Appendix.

An investigation of the dependence of  $|\nabla(\mathbf{E} \cdot \mathbf{E})|$  on a characteristic length scale of the system,  $L_e$  reveals some interesting behavior. Shown in Fig. 6 is a plot of  $|\nabla(\mathbf{E} \cdot \mathbf{E})|$  as a function of electrode width,  $w$ , at test height,  $h$ , of  $1 \mu\text{m}$  for various applied voltages.

For all of the applied voltages tested, a power law fit shows that  $|\nabla(\mathbf{E} \cdot \mathbf{E})|$  scales as  $w^{-1.76}$  with a correlation coefficient 1. Based on the scaling estimate given in Eq. (8), a power law fit was expected to yield an inverse cubic depen-

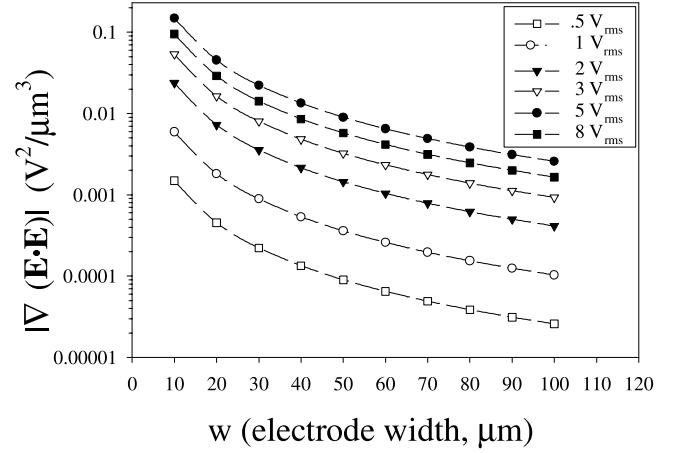


FIG. 6. Gradient in electric field intensity as a function of electrode width  $w$ . The electrode widths  $w$  and edge-to-edge spacing  $s$  are equal and range from  $10 \mu\text{m}$  to  $100 \mu\text{m}$ . The applied voltage ranges from  $0.5$  to  $8 V_{rms}$ .

dence on the electrode width. However, the curve fits show that for a fixed test height the electric field intensity, and therefore the DEP force, is a function of more than one length scale in the system.

By closely examining the analytic expressions given in the Appendix for the case when the test height is less than the electrode width, order of magnitude estimates of these expressions reveal that there are three dominant contributions,

$$|\nabla(\mathbf{E} \cdot \mathbf{E})| \sim O\left(\frac{1}{w^3}\right), O\left(\frac{1}{w h^2}\right), \text{ and } O\left(\frac{1}{h^3}\right). \quad (10)$$

Only the first term predicts the expected inverse cubic dependence on the electrode width. The other two terms however predict that the magnitude of the gradient in the electric field intensity is also dependent on the choice of the test height,  $h$ . Consequently, at the test height used in these studies,  $1 \mu\text{m}$ , the dependence on the electrode width should be in the range between  $w^{-1}$  and  $w^{-3}$ ; hence, the dependence predicted by the curve fitting is entirely consistent with the order of magnitude estimates given in Eq. (10).

### C. Dependence on electrode spacing

The final parameter investigated in this paper is the edge-to-edge spacing between electrodes,  $s$ . In general, as the electrode spacing increases the DEP force decreases. Here 4 electrode widths were chosen and the magnitude of the gradient of the electric field intensity is calculated for various  $s$ . The results were normalized by the magnitude of the gradient found when  $s = w$ . In Fig. 7, the results are plotted as a function of the ratio of the spacing to electrode width,  $s/w$ .

Consistent with the dependence on  $w$  as predicted by curve fitting the data in Fig. 5, the normalized data collapses onto one curve. Fitting the data to a power law produces the following relationship for  $|\nabla(\mathbf{E} \cdot \mathbf{E})|/|\nabla(\mathbf{E} \cdot \mathbf{E})|_{s/w=1} \sim (s/w)^{-1.69}$ . As  $s$  is decreased below  $2w$  the gradient in the

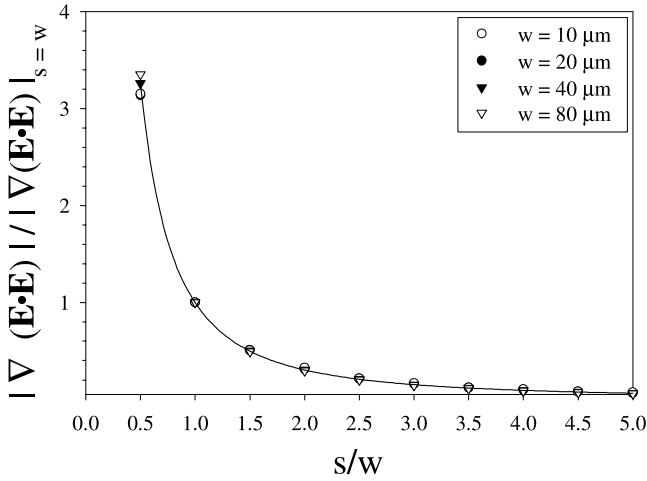


FIG. 7. Normalized magnitude in the gradient in electric field intensity as a function of the spacing between electrodes. The magnitude in the gradient in the electric field intensity is normalized by the corresponding value when the electrode widths  $w$  and spacing  $s$  are equal. The electrode widths considered are 10, 20, 40, and 80  $\mu\text{m}$ , and the applied voltage is  $5 V_{rms}$ .

electric field intensity increases exponentially. This marked increase results from the stronger near-field electrode-electrode interactions. For spacings greater than or equal to  $2w$ , the magnitude of the gradient in the electric field intensity is much less than the magnitude when  $s/w=1$ . This result reveals that for all electrode widths the electric field intensity exhibits the same dependence on the edge to edge spacing  $s$  between adjacent electrodes. This result also demonstrates that the spacing between electrodes is an important design consideration when seeking a desired dielectrophoretic force.

#### IV. CONCLUSIONS

The use of the two-dimensional half-space Green's function, Eq. (2), with a linear approximation for the surface

potential in regions between electrodes yields an identical expression for the electric potential as Wang *et al.* [5]. This common result validates our respective approaches. Characterization of the gradient in the electric field intensity as a function of the applied voltage reveals the expected  $V^2$  dependence as predicted by the order of magnitude estimate given in Eq. (8). The data however did not reveal a cubic dependence on a particular length scale in the system, the electrode width, as suggested by Eq. (8). Order of magnitude estimates, based on the analytic results from the Appendix, given in Eq. (10) show that the expected dependence on the electrode width  $w$  actually falls in the range between  $w^{-1}$  and  $w^{-3}$ . These estimates are consistent with the dependence found from curve fits of the data. For all electrode widths, the magnitude in the gradient in the electric field intensity shows the same dependence on the spacing between adjacent electrodes; furthermore, when the spacing between adjacent electrodes is reduced below two electrode widths, the magnitude increases exponentially.

#### ACKNOWLEDGMENTS

One of the authors (D.C.) would like to thank G. Cooper of the Center for Microtechnology at LLNL for useful discussions. This work was motivated by interactions within the DARPA BioFlips program and was partially funded through the Laboratory Directed Research and Development program at Lawrence Livermore National Laboratory. This research was conducted under the auspices of the U.S. Department of Energy by Lawrence Livermore National Laboratory, Contract No. W-7405-ENG-48. The authors would, also, like to thank the Lawrence Livermore computing facilities for computational time.

#### APPENDIX

The components of the electric field are obtained by taking the gradient of  $-\psi(x_1, x_3)$ . For example,  $E_1 = -\partial\psi(x_1, x_3)/\partial x_1$ . The precise expressions for  $E_1$  and  $E_3$  are given below in Eqs. (A1) and (A2).

$$\begin{aligned}
 E_1 = & \frac{1}{\pi} \sum_{j=1}^N \psi_e \left( \frac{x_3 - x_{3_0}}{[x_3 - x_{3_0}]^2 + [x_1 - b_j]^2} - \frac{x_3 - x_{3_0}}{[x_3 - x_{3_0}]^2 + [x_1 - a_j]^2} \right) + \frac{1}{\pi} \sum_{j=1}^{N-1} \left\{ \psi_g(x_1) \left[ \frac{x_3 - x_{3_0}}{(x_3 - x_{3_0})^2 + (x_1 - a_{j+1})^2} \right. \right. \\
 & \left. \left. - \frac{x_3 - x_{3_0}}{(x_3 - x_{3_0})^2 + (x_1 - b_j)^2} \right] + C_2 \left( \arctan \left[ \frac{x_1 - a_{j+1}}{x_3 - x_{3_0}} \right] - \arctan \left[ \frac{x_1 - b_j}{x_3 - x_{3_0}} \right] \right) - C_2(x_3 - x_{3_0}) \left[ \frac{x_1 - a_{j+1}}{(x_3 - x_{3_0})^2 + (x_1 - a_{j+1})^2} \right. \right. \\
 & \left. \left. - \frac{x_1 - b_j}{(x_3 - x_{3_0})^2 + (x_1 - b_j)^2} \right] \right\}. \tag{A1}
 \end{aligned}$$

Correspondingly, the  $x_3$  component or  $E_3$  is given by

$$\begin{aligned}
E_3 = & \frac{1}{\pi} \sum_{j=1}^N \psi_e \left( \frac{x_1 - a_j}{[x_3 - x_{3_0}]^2 + [x_1 - a_j]^2} - \frac{x_1 - b_j}{[x_3 - x_{3_0}]^2 + [x_1 - b_j]^2} \right) + \frac{1}{\pi} \sum_{j=1}^{N-1} \left\{ \psi_g(x_1) \left[ \frac{x_1 - b_j}{(x_3 - x_{3_0})^2 + (x_1 - b_j)^2} \right. \right. \\
& - \left. \frac{x_1 - a_{j+1}}{(x_3 - x_{3_0})^2 + (x_1 - a_{j+1})^2} \right] - C_2 (x_3 - x_{3_0})^2 \left[ \frac{1}{(x_3 - x_{3_0})^2 + (x_1 - a_{j+1})^2} - \frac{1}{(x_3 - x_{3_0})^2 + (x_1 - b_j)^2} \right] \\
& \left. - \frac{C_2}{2} \ln \left[ \frac{(x_3 - x_{3_0})^2 + (x_1 - a_{j+1})^2}{(x_3 - x_{3_0})^2 + (x_1 - b_j)^2} \right] \right\}. \tag{A2}
\end{aligned}$$

In accordance with Eq. (7), the components of the gradient in the electric field intensity are made up of the first partials of the components of the electric field. The partial derivative of  $E_1$  with respect to  $x_1$  is

$$\begin{aligned}
\frac{\partial E_1}{\partial x_1} = & \frac{2(x_3 - x_{3_0})}{\pi} \sum_{j=1}^N \psi_e \left( \frac{x_1 - a_j}{\{[x_3 - x_{3_0}]^2 + [x_1 - a_j]^2\}^2} - \frac{x_1 - b_j}{\{[x_3 - x_{3_0}]^2 + [x_1 - b_j]^2\}^2} \right) + \frac{1}{\pi} \sum_{j=1}^{N-1} \left\{ 2(x_3 - x_{3_0}) \psi_g(x_1) \right. \\
& \times \left( \frac{x_1 - b_j}{\{[x_3 - x_{3_0}]^2 + [x_1 - b_j]^2\}^2} - \frac{x_1 - a_{j+1}}{\{[x_3 - x_{3_0}]^2 + [x_1 - a_{j+1}]^2\}^2} \right) + 2 C_2 \left( \frac{x_3 - x_{3_0}}{[x_3 - x_{3_0}]^2 + [x_1 - a_{j+1}]^2} \right. \\
& \left. - \frac{x_3 - x_{3_0}}{[x_3 - x_{3_0}]^2 + [x_1 - b_j]^2} \right) - C_2 (x_3 - x_{3_0}) \left[ \frac{(x_3 - x_{3_0})^2 - (x_1 - a_{j+1})^2}{\{(x_3 - x_{3_0})^2 + (x_1 - a_{j+1})^2\}^2} \right] - \left. \left[ \frac{(x_3 - x_{3_0})^2 - (x_1 - b_j)^2}{\{(x_3 - x_{3_0})^2 + (x_1 - b_j)^2\}^2} \right] \right\}, \tag{A3}
\end{aligned}$$

and the partial of  $E_3$  with respect to  $x_3$  is given by

$$\begin{aligned}
\frac{\partial E_3}{\partial x_3} = & \frac{2(x_3 - x_{3_0})}{\pi} \sum_{j=1}^N \psi_e \left( \frac{x_1 - b_j}{\{[x_3 - x_{3_0}]^2 + [x_1 - b_j]^2\}^2} - \frac{x_1 - a_j}{\{[x_3 - x_{3_0}]^2 + [x_1 - a_j]^2\}^2} \right) + \frac{1}{\pi} \sum_{j=1}^{N-1} \left\{ 2(x_3 - x_{3_0}) \psi_g(x_1) \right. \\
& \times \left[ \frac{x_1 - a_{j+1}}{\{(x_3 - x_{3_0})^2 + (x_1 - b_{j+1})^2\}^2} - \frac{x_1 - b_j}{\{(x_3 - x_{3_0})^2 + (x_1 - b_j)^2\}^2} \right] \\
& - 2 C_2 (x_3 - x_{3_0})^3 \left[ \frac{1}{\{(x_3 - x_{3_0})^2 + (x_1 - b_j)^2\}^2} - \frac{1}{\{(x_3 - x_{3_0})^2 + (x_1 - a_{j+1})^2\}^2} \right] - 3 C_2 (x_3 - x_{3_0}) \\
& \times \left. \left[ \frac{1}{(x_3 - x_{3_0})^2 + (x_1 - a_{j+1})^2} - \frac{1}{(x_3 - x_{3_0})^2 + (x_1 - b_j)^2} \right] \right\}. \tag{A4}
\end{aligned}$$

The partial of  $E_3$  with respect to  $x_1$  is given by

$$\begin{aligned}
\frac{\partial E_3}{\partial x_1} = & \frac{1}{\pi} \sum_{j=1}^N \psi_e \left( \frac{[x_3 - x_{3_0}]^2 - [x_1 - a_j]^2}{\{[x_3 - x_{3_0}]^2 + [x_1 - a_j]^2\}^2} - \frac{[x_3 - x_{3_0}]^2 - [x_1 - b_j]^2}{\{[x_3 - x_{3_0}]^2 + [x_1 - b_j]^2\}^2} \right) + \frac{1}{\pi} \sum_{j=1}^{N-1} \left\{ \psi_g(x_1) \left[ \frac{(x_3 - x_{3_0})^2 + (x_1 - b_j)^2}{\{(x_3 - x_{3_0})^2 + (x_1 - b_j)^2\}^2} \right. \right. \\
& - \left. \frac{(x_3 - x_{3_0})^2 - (x_1 - a_{j+1})^2}{\{(x_3 - x_{3_0})^2 + (x_1 - a_{j+1})^2\}^2} \right] + 2 C_2 \left( \frac{x_1 - b_j}{[x_3 - x_{3_0}]^2 + [x_1 - b_j]^2} - \frac{x_1 - a_{j+1}}{[x_3 - x_{3_0}]^2 + [x_1 - a_{j+1}]^2} \right) \\
& \left. - 2 C_2 (x_3 - x_{3_0})^2 \left[ \frac{x_1 - b_j}{\{(x_3 - x_{3_0})^2 + (x_1 - b_j)^2\}^2} - \frac{x_1 - a_{j+1}}{\{(x_3 - x_{3_0})^2 + (x_1 - a_{j+1})^2\}^2} \right] \right\}. \tag{A5}
\end{aligned}$$

Furthermore, the partial of  $E_1$  with respect to  $x_3$  is

$$\begin{aligned}
\frac{\partial E_1}{\partial x_3} = & \frac{1}{\pi} \sum_{j=1}^N \psi_e \left( \frac{[x_3 - x_{3_0}]^2 - [x_1 - a_j]^2}{\{[x_3 - x_{3_0}]^2 + [x_1 - a_j]^2\}^2} - \frac{[x_3 - x_{3_0}]^2 - [x_1 - b_j]^2}{\{[x_3 - x_{3_0}]^2 + [x_1 - a_j]^2\}^2} \right) + \frac{1}{\pi} \sum_{j=1}^{N-1} \left\{ \psi_g(x_1) \left[ \frac{(x_3 - x_{3_0})^2 - (x_1 - b_j)^2}{\{(x_3 - x_{3_0})^2 + (x_1 - b_j)^2\}^2} \right. \right. \\
& - \left. \frac{(x_3 - x_{3_0})^2 - (x_1 - a_{j+1})^2}{\{(x_3 - x_{3_0})^2 + (x_1 - a_{j+1})^2\}^2} \right] + 2 C_2 \left( \frac{x_1 - b_j}{[x_3 - x_{3_0}]^2 + [x_1 - b_j]^2} - \frac{x_1 - a_{j+1}}{[x_3 - x_{3_0}]^2 + [x_1 - a_{j+1}]^2} \right) \\
& \left. - 2 C_2 (x_3 - x_{3_0})^2 \left[ \frac{x_1 - b_j}{\{(x_3 - x_{3_0})^2 + (x_1 - b_{j+1})^2\}^2} - \frac{x_1 - a_{j+1}}{\{(x_3 - x_{3_0})^2 + (x_1 - a_{j+1})^2\}^2} \right] \right\}. \tag{A6}
\end{aligned}$$

In accordance with the Swartz relationship, [4] the cross terms,  $\partial E_3 / \partial x_1$  and  $\partial E_1 / \partial x_3$ , are equivalent.

- 
- [1] H.A. Pohl, *Dielectrophoresis* (Cambridge University Press, New York, 1978).
- [2] Thomas B. Jones, *Electromechanics of Particles* (Cambridge University Press, New York, 1995).
- [3] X.-B Wang Y. Huang, F.F. Becker, and P.R.C. Gascoyne, J. Phys. D **27**, 1571 (1994).
- [4] X.-B. Wang Y. Huang, J.P.H. Burt, G.H. Markx, and R. Pethig, J. Phys. D **26**, 1278 (1993).
- [5] X. Wang, X.B. Wang, F.F. Becker, and Peter R.C. Gascoyne, J. Phys. D **29**, 1649 (1996).
- [6] P.R.C. Gascoyne, J. Noshari, F.F. Becker, and R. Pethig, IEEE Trans. Ind. Appl. **30**, 829 (1994).
- [7] X.-B. Wang, Y. Huang, P.R.C. Gascoyne, F.F. Becker, R. Holz, and R. Pethig, *Biochim. Biophys. Acta* **1193**, 330 (1994).
- [8] M. Garcia and D. S. Clague, J. Phys. D **33**, 1747 (2000).
- [9] P. M. Morse and H. Feshbach, *Methods of Theoretical Physics, Part 1* (McGraw-Hill, New York, 1953).
- [10] R. Miles, P. Belgrader, K. Bettencourt, J. Hamilton, and S. Nasarabadi, in *Proceedings of the International Mechanical Engineering Congress and Exposition 299 Microfluidics Symposium*, Nashville, TN, 1999, edited by A.P. Lee *et al.* (ASME International, New York, 1999).
- [11] P.G. Saffman, J. Fluid Mech. **22**, 385 (1965).
- [12] A.S. Bahaj and A.G. Bailey, J. Phys. D: Appl. Phys. **12**, L109 (1979).